RSC Advances

PAPER

View Article Online
View Journal | View Issue

Cite this: *RSC Adv.*, 2026, **16**, 25385

Structural engineering of cattle manure-derived carbon for lithium–sulfur batteries

Peng Li,*[ab] Yingjie Liu,[b] Yongzhen Ma,[b] Zhicheng Zhao[b] and Zheng Zhang[b]

The large-scale generation and disposal pressure of cattle manure make its high-value conversion an important environmental and resource-utilization issue, and developing low-cost sulfur hosts from this waste is an attractive strategy for lithium–sulfur battery materials. However, the intrinsic relationship among carbonization temperature, framework ordering, pore architecture, surface heteroatoms, and electrochemical response within a single precursor system remains insufficiently understood. Here, a unified pretreatment route comprising water washing, alkali treatment, acid hydrolysis, and oxidative stabilization was combined with carbonization at 650–1050 °C to prepare a series of cattle-manure-derived carbons. The sample obtained at 1000 °C (AH-1000) exhibits a relatively complete three-dimensional conductive framework, a balanced micro/mesoporous texture, and moderate retention of polar N/O sites. As a sulfur host, AH-1000 delivers an initial specific capacity of 690 mAh g^{-1} at 0.1C, together with better rate response and more stable cycling over 100 cycles than the other temperature-series samples. These results indicate that the electrochemical response of cattle-manure-derived carbons is closely related to the temperature-dependent balance among electrical conductivity, pore structure, and surface-active-site retention. Nevertheless, owing to the intrinsic limitations of the cattle-manure precursor, these carbons still show a lower specific surface area and a less developed pore structure than highly active carbon hosts such as Ketjen Black, resulting in relatively limited sulfur-storage capability. This study therefore provides a structural basis for the further optimization of cattle-manure-derived carbon materials.

Received 25th February 2026
Accepted 1st May 2026

DOI: 10.1039/d6ra01639a

rsc.li/rsc-advances

1. Introduction

Cattle manure is generated in large quantities during livestock farming, and its improper treatment can aggravate environmental disposal pressure while wasting a potentially carbon-rich resource. In recent years, biomass wastes have attracted sustained attention as precursors for functional carbon materials because they are renewable, low-cost, and environmentally benign.[1,2] Compared with rice husks, straw, and woody fibers, cattle manure offers both practical and structural advantages: it is abundant, under disposal pressure, and rich in cellulose, hemicellulose, and lignin. After ruminant digestion, the remaining organic fraction retains a relatively compact fibrous scaffold together with inherent N, O, and S species, providing a natural basis for self-doped carbon materials.[3,4] Converting cattle manure from a low-value agricultural residue into electrochemically active carbon is therefore relevant to both waste valorization and sustainable energy-storage materials. Recent studies further show that ultramicropore regulation and interfacial adsorption engineering can strongly influence mass transport and interfacial interactions in biomass-derived carbons.[5,6] From a broader sustainability perspective, waste valorization, battery-related waste management, sulfur-containing resource conversion, and low-carbon multi-energy optimization are increasingly discussed as interconnected research themes.[7,8] In addition, self-etching/graphitization regulation and structured biomass-derived carbons, such as carbon aerogels, have demonstrated the tunability of carbon-framework design.[9,10]

For sulfur-host design in lithium–sulfur batteries, recent studies have mainly followed three directions: increasing specific surface area and pore volume through activation, strengthening polysulfide adsorption by N/O/S heteroatom regulation, and introducing polar or catalytic components to accelerate polysulfide conversion.[11,12] Against this background, simply replacing one biomass precursor with another offers limited novelty. The more meaningful question is how carbonization temperature, within the same precursor system and without additional catalytic components, governs the structural parameters that jointly determine sulfur utilization, reaction kinetics, and cycling stability. Recent reports on dynamic Ni–N4 sites further indicate that high-performance Li–S systems usually rely on multidimensional synergistic design

[a]*College of Energy Science and Engineering, Taiyuan University of Science and Technology, Taiyuan 030024, China. E-mail: lipeng_ty@tyust.edu.cn*
[b]*College of Chemical Engineering and Technology, Taiyuan University of Science and Technology, Taiyuan 030024, China*

rather than pore structure alone.[13,14] Meanwhile, thermo-electrochemical coupling and state-estimation studies remind us that material design must ultimately be interpreted under realistic operating conditions and full-cell constraints.[15,16] At the cell level, the lithium metal anode, the polysulfide shuttle, and cathode-electrolyte coupling remain major barriers to energy density and cycle life.[17,18] Accordingly, nanostructured carbon hosts, polar hosts, MXene-based hosts, and conductive nitride/graphene composites have been widely explored to strengthen polysulfide immobilization and conversion.[19,20] Reviews from the biomass-carbon perspective likewise emphasize the importance of precursor chemistry and structural regulation.[21]

More specifically, high-performing carbon hosts commonly rely on high-surface-area activation, hierarchical pore reconstruction, and synergy between polar sites and catalytic centers to raise sulfur utilization and accelerate polysulfide conversion.[22,23] No additional catalytic component or secondary synthetic route was introduced in the present work. Instead, the mechanistic focus is placed on what carbonization temperature changes within a single cattle-manure precursor system. Interlayer design, single-atom sites, electrocatalytic promotion of sulfur redox, and heterostructured hosts have all been proven effective for boosting Li–S kinetics and durability.[24,25] These studies underscore the performance gap between simple carbon hosts and advanced multifunctional systems, and they also help define the boundary conditions under which the present temperature-series study should be interpreted.[26,27]

Based on these considerations, cattle manure was selected as a model biomass precursor with inherent self-doping potential. Under identical pretreatment conditions, only the carbonization temperature was varied to produce AH-650, AH-850, AH-1000, and AH-1050. Their morphology, crystal structure, pore structure, surface chemistry, and electrochemical response were then compared systematically. The aim is to clarify the intrinsic temperature–structure–performance relationship in cattle-manure-derived carbons, identify the temperature window that best balances conductive framework construction, pore integrity, and polar-site retention, and define the performance boundary of this low-cost biomass route relative to advanced catalytic or highly activated sulfur hosts.

2. Experimental section

2.1. Materials and reagents

Pure dried cattle manure was collected locally from Shanxi Province. Sodium hydroxide (NaOH) was purchased from Tianjin Comio Chemical Reagent Co., Ltd. Sulfuric acid (H_2SO_4) solution (98 wt%) was obtained from Sichuan Xilong Scientific Co., Ltd. *N*-Methyl-2-pyrrolidone (NMP) and poly(vinylidene fluoride) (PVDF) binder were sourced from Tianjin Dingshengxin Chemical Co., Ltd and Kelude Co., Ltd, respectively. The lithium–sulfur battery electrolyte (1 M lithium bis(trifluoromethanesulfonyl)imide (LiTFSI) in a mixed solvent of 1,2-dimethoxyethane (DME) and 1,3-dioxolane (DOL) (1 : 1 by volume) with 1 wt% $LiNO_3$ additive) was purchased from Shanghai Macklin Biochemical Technology Co., Ltd.

2.2. Preparation of the carbon precursor

The dried cattle manure was first crushed into fine particles using a pulverizer. To remove sand and soil impurities, the particles were thoroughly washed with tap water and then dried in an oven at 70 °C until a constant weight was achieved, yielding crude fibers. Subsequently, 10 g of the crude fibers were mixed with a 3 wt% NaOH aqueous solution at a solid-to-liquid ratio of 1 : 20 (g : mL). The mixture was stirred in a water bath at 90 °C for 30 min. The resulting product was then washed and filtered repeatedly until the filtrate reached neutral pH, followed by drying at 70 °C to constant weight. The dried solid was ball-milled for 48 h. Next, 4 g of the ball-milled sample was added to 80 mL of a 3 wt% H_2SO_4 solution. The mixture was transferred into a Teflon-lined autoclave, sealed tightly, and heated in a homogeneous reactor at 150 °C for 2 h. After cooling to room temperature, the product was collected, washed to neutrality, filtered, and dried at 70 °C to obtain the final carbon precursor.

2.3. Synthesis of porous carbon materials

One gram of the precursor was placed in a ceramic boat and subjected to oxidative stabilization in a muffle furnace. The temperature was raised to 275 °C and held for 12 h. After cooling to room temperature, the stabilized sample was transferred to a tube furnace for carbonization under a continuous nitrogen (N_2) flow. The temperature was increased to the target value (650, 850, 1000, or 1050 °C) at a heating rate of 5 °C min^{-1}, maintained for 2 h, and then allowed to cool naturally to room temperature. The resulting carbon materials obtained at different temperatures are denoted as AH-650, AH-850, AH-1000, and AH-1050, respectively. The overall preparation route from raw cattle manure to porous carbon is shown in Fig. 1.

2.4. Material characterization

The morphology and microstructure of the samples were observed using field-emission scanning electron microscopy (FESEM, JSM-7900F, JEOL). Crystal structure analysis was performed by X-ray diffraction (XRD) on a D8 Advance diffractometer (Bruker) with Cu Kα radiation ($\lambda = 0.15405$ nm). Surface functional groups were identified using Fourier-transform infrared spectroscopy (FT-IR, Thermo Scientific Nicolet iS50) in the wavenumber range of 500–4000 cm^{-1}. The specific surface area and pore size distribution were determined by nitrogen adsorption–desorption measurements at 77 K using a Micromeritics ASAP 2460 analyzer. Surface elemental composition and chemical states were analyzed by X-ray photoelectron spectroscopy (XPS, Thermo Scientific K-Alpha). Raman spectroscopy was conducted on a Bruker SENTERRA confocal Raman microscope with a 532 nm laser excitation source.

2.5. Sulfur cathode preparation and electrochemical characterization

First, the porous carbon host and nano-sulfur powder (Fig. S3) were thoroughly mixed by grinding at a mass ratio of 3 : 7. The resulting mixture was then blended with conductive carbon

Fig. 1 Schematic illustration of the preparation route for cattle-manure-derived carbon hosts for lithium–sulfur batteries, including water washing, alkali treatment, acid hydrolysis, oxidative stabilization, and carbonization at 650, 850, 1000, or 1050 °C.

black and PVDF binder at a mass ratio of 8 : 1 : 1, followed by the dropwise addition of an appropriate amount of NMP to form a homogeneous slurry. The slurry was coated onto aluminum foil using a doctor-blade method and dried overnight in a vacuum oven at 60 °C. The dried electrode was punched into circular disks with a diameter of 12 mm to serve as the cathode. The sulfur loading in each cathode was about 0.9 mg, corresponding to an average areal sulfur loading of about 0.80 mg cm^{-2}. CR2032 coin cells were assembled in an argon-filled glove box with H_2O and O_2 levels below 0.1 ppm. The cell consisted of the as-prepared cathode, a Celgard 2400 separator, a lithium metal anode, and the purchased lithium–sulfur electrolyte. The lithium foil had a thickness of 0.5 mm and a diameter of 15.8 mm. A total of 70 μL electrolyte was added to each cell, corresponding to an electrolyte/sulfur (E/S) ratio of about 77.8 μL mg^{-1}. After assembly, the cells were allowed to rest for 12 h before electrochemical testing.

Galvanostatic charge–discharge measurements, including cycling performance and rate-capability evaluation, were carried out on a LAND battery testing system (CT2001A, CT3002A) within a voltage window of 1.7–2.8 V (*vs.* Li^+/Li). Cyclic voltammetry (CV) and electrochemical impedance spectroscopy (EIS) were performed using a Pine WaveDriver200 electrochemical workstation. CV was recorded over 1.7–2.8 V at different scan rates. EIS was measured in the frequency range of 10^{-1} to 10^6 Hz with an AC perturbation amplitude of 5 mV.

3. Results and discussion

3.1. Material preparation and structural design

This study aims to convert cattle manure into functional carbon host materials suitable for lithium–sulfur batteries through a systematic chemical–thermal treatment route. The core of this strategy lies in reconstructing the precursor structure and using carbonization temperature to achieve precise regulation of the final material properties. As illustrated in Fig. 1, the preparation starts from the pretreatment of dried cattle manure: crushing and water washing were first carried out to remove inorganic impurities, followed by a key alkali treatment (NaOH, 90 °C) and acid hydrolysis (dilute H_2SO_4, 150 °C). These two steps sequentially act on lignin, hemicellulose, and cellulose in the biomass, disrupt the dense cross-linked structure, and induce partial depolymerization or removal, thereby generating initial pores and establishing a porous precursor basis for subsequent carbonization.[28] This was followed by oxidative stabilization in air at 275 °C, aiming to improve the thermal stability of the precursor by introducing oxygen-containing cross-linking bonds and thus avoid structural melting and collapse during later high-temperature treatment.[29] Finally, high-temperature carbonization (650–1050 °C) was conducted under a nitrogen atmosphere. This step plays a decisive role in the final properties because temperature directly affects the ordering of the carbon framework, the evolution of pore structure, and the retention state as well as chemical environment of intrinsic heteroatoms (N and O).[30] Importantly, the pretreatment route was kept identical in this work and only the carbonization temperature was varied. The structural differences discussed below can therefore be attributed more directly to temperature-governed changes in framework ordering, pore structure, and surface chemistry, rather than to multivariable modification strategies. This route uses widely available raw materials and a relatively simple process, indicating some scale-up potential; however, the acid/alkali treatments and repeated washing steps still need to be simplified in future work to better balance cost, environmental burden, and batch stability.

3.2. Evolution of morphology and crystal structure

3.2.1. Micromorphology analysis (SEM). The morphological evolution of the materials from raw cattle manure to the final carbonized products was systematically tracked by scanning electron microscopy (SEM), as shown in Fig. 2. Raw cattle manure (Fig. 2a) exhibits a dense, rough, fibrous block-like structure. After alkali treatment (Fig. 2b) and acid hydrolysis (Fig. 2c), components such as hemicellulose and lignin were effectively stripped and depolymerized, making the surface looser and creating obvious cracks and initial pores, thereby establishing structural channels for the subsequent carbonization process.[31] After oxidative stabilization (Fig. 2d), the porous precursor framework was further consolidated.

Carbonization temperature plays a decisive role in the formation of the final morphology. The sample obtained at 650 °C, AH-650 (Fig. 2e), had already been carbonized, but still mainly retained a fibrous morphology and showed limited pore development. AH-850 prepared at 850 °C (Fig. 2f) began to form a comparatively optimized porous structure. Notably, AH-1000 carbonized at 1000 °C (Fig. 2g) constructed a robust three-dimensional interconnected carbon network, which is beneficial for forming continuous electron-transport pathways and promoting electrolyte infiltration.[32] When the temperature was further increased to 1050 °C, the carbon skeleton of AH-1050 (Fig. 2h) underwent obvious shrinkage and densification, accompanied by a reduction in macroporous structures. This suggests that its specific surface area and porosity may decrease, which would be unfavorable for sulfur loading and effective confinement of polysulfides.[33]

3.2.2. Analysis of crystal structure and degree of ordering (XRD and Raman). To further elucidate the effect of carbonization temperature on the microcrystalline structure of cattle-manure-derived carbons, X-ray diffraction (XRD) and Raman spectroscopy were carried out, as shown in Fig. 3. All samples exhibit a broad diffraction feature around 23°, characteristic of disordered carbon. A gradually emerging feature near 26.5° can be assigned to graphite-like (002) stacking, whereas a weak broad band near 43°, when visible, is attributable to the (100) plane; these assignments are consistent with graphite PDF #41-1487. With increasing carbonization temperature, the feature near 26.5° becomes progressively clearer and is most evident for AH-1000, indicating more developed local graphite-like stacking or graphitic microdomains rather than complete graphitization. Such evolution is beneficial for improving intrinsic electronic conductivity and thereby facilitating electron transport during sulfur redox.[34]

Raman spectroscopy further clarifies the evolution of framework ordering and defect chemistry. All samples display the characteristic D band (~1350 cm^{-1}) and G band (~1580 cm^{-1}) associated with disordered and graphitic sp^2 carbon, respectively. The I_D/I_G ratio first increases and then decreases slightly with temperature, from 0.94 (AH-650) to 1.09 (AH-850), 1.10 (AH-1000), and 1.01 (AH-1050). I_D/I_G should not be interpreted as a single-valued measure of graphitization; instead, it reflects the overall balance among ordered sp^2 domains, defect density, and edge sites. The comparatively high I_D/I_G value of AH-1000 indicates that this sample retains abundant defects and active boundaries while preserving an electrically percolated framework, which is favorable for polysulfide adsorption and interfacial sulfur redox.[35] By contrast, further structural rearrangement in AH-1050 reduces the density of defect sites; although local ordering is improved, surface-active sites are lost at the same time. Taken together, the XRD and Raman results indicate that 1000 °C affords the most suitable balance between partial ordering and moderate defect retention.

3.2.3. Quantitative analysis of porous structure (BET). To quantitatively reveal the regulating effect of carbonization temperature on the pore structure of cattle manure-derived carbons, N_2 adsorption–desorption measurements were conducted. As shown in Fig. 4, all samples exhibit typical type-IV adsorption isotherms with H3 hysteresis loops, indicating the

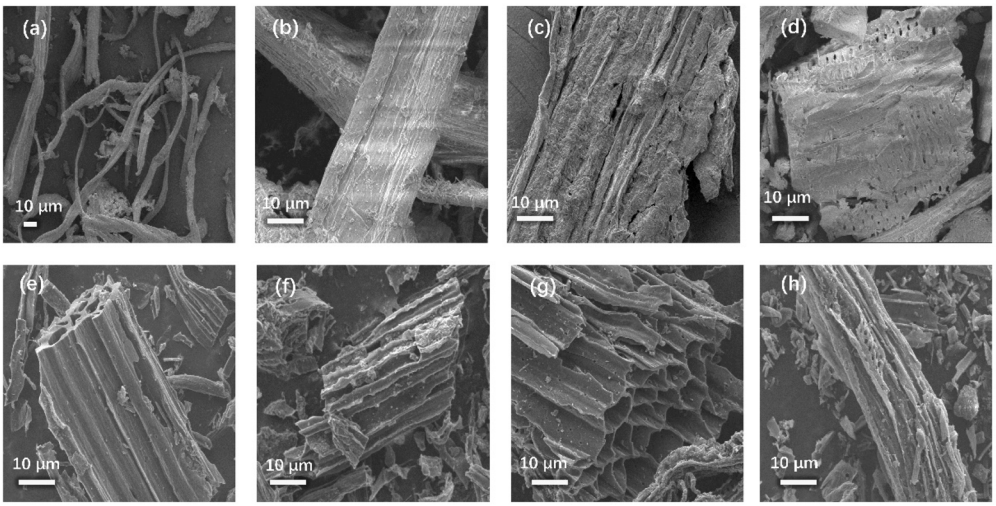

Fig. 2 SEM images showing the morphological evolution of cattle manure during pretreatment and carbonization: (a) raw cattle manure, (b) alkali-treated precursor, (c) acid-hydrolyzed precursor, (d) oxidatively stabilized precursor, (e) AH-650, (f) AH-850, (g) AH-1000, and (h) AH-1050.

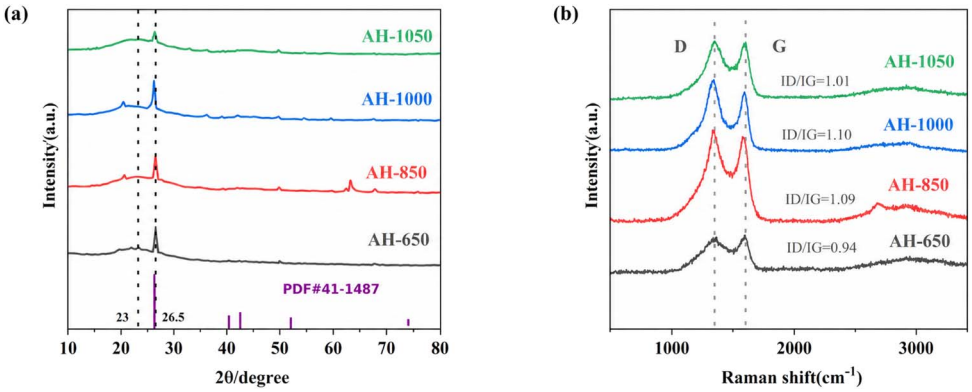

Fig. 3 Structural characterization of cattle-manure-derived carbons carbonized at different temperatures: (a) XRD patterns with the graphite reference card (PDF #41-1487) and the characteristic positions of disordered carbon, graphite-like (002) stacking, and the (100) plane; (b) Raman spectra showing the D and G bands used to evaluate defect density and carbon-framework ordering.

presence of slit-shaped mesopores (2–50 nm) formed by the stacking of sheet-like particles. The pore size distribution (PSD) curves further confirm the existence of continuous hierarchical pore structures ranging from micropores (<2 nm) to mesopores. Quantitative data (Table 1) show that although the BET specific surface areas of the samples carbonized at different temperatures are close, all remaining within 72–78 $m^2 g^{-1}$, systematic differences still exist in the intrinsic features of their pore structures. Notably, this specific-surface-area level is still far lower than that of Ketjen Black or highly activated biomass-derived carbon hosts, indicating that the present route establishes only a modest hierarchical pore framework. This limited pore development is also an important reason why the subsequent electrochemical performance remains moderate.

AH-1000 possesses the smallest average pore size (17.6 nm) and a moderate micropore area, indicating a more compact and balanced pore structure. For sulfur hosts in lithium–sulfur batteries, such an optimized hierarchical pore synergy is crucial. Abundant micropores can provide a relatively high surface area and defect sites, serving as the first barrier for the physical confinement and chemical adsorption of polysulfides.[36] A well-developed mesoporous network offers the

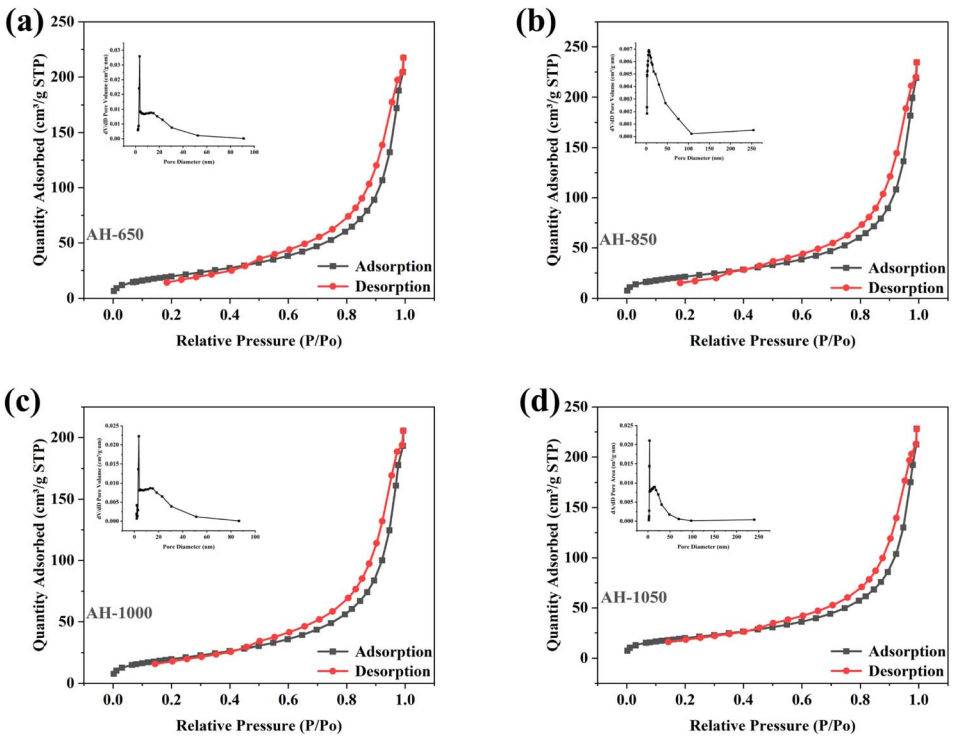

Fig. 4 N_2 adsorption–desorption isotherms and pore size distribution of the materials carbonized at different temperatures: (a) 650 °C carbonization, (b) 850 °C carbonization, (c) 1000 °C carbonization, and (d) 1050 °C carbonization.

Table 1 BET data of the materials carbonized at different temperatures

Thermophysical properties	AH-650	AH-850	AH-1000	AH-1050
BET surface area ($m^2\ g^{-1}$)	73.7867	77.9279	72.2506	72.3444
Micropore area ($m^2\ g^{-1}$)	82.9095	80.0506	73.7911	74.4073
Average pore size (nm)	18.2353	18.6273	17.6047	19.5263

main space for sulfur loading and also provides key mass-transport channels for the dissolution and migration of polysulfides. In addition, the relatively small average pore size, together with the three-dimensional network skeleton observed by SEM, helps construct more tortuous diffusion pathways, thereby strengthening the physical blocking effect against polysulfide shuttling[37] and promoting effective electrolyte wetting. By contrast, AH-1050 exhibits a larger average pore size without a significant increase in micropore area, suggesting pore coarsening together with partial fusion or collapse of micropores at 1050 °C. This is consistent with the densification trend observed by SEM. Such pore-structure deterioration weakens physical confinement; together with the generally low pore volume and specific surface area, it ultimately limits sulfur loading and the restraint of soluble intermediates.

3.3. Analysis of surface chemical states and elemental composition

3.3.1. Analysis of surface chemical states (XPS). To clarify the effect of carbonization temperature on surface chemistry, X-ray photoelectron spectroscopy (XPS) was carried out. The XPS survey spectra (Fig. 5) show characteristic C 1s, O 1s, and N 1s signals for all samples, directly confirming the successful preparation of N,O-co-doped carbon materials from the cattle manure precursor. More importantly, these N/O species provide polar surface sites that can interact with lithium polysulfides. As the carbonization temperature increases from 650 to 1050 °C, the relative intensities of the O 1s and N 1s signals decrease systematically, with the strongest attenuation observed for AH-1050. This indicates that excessively high temperature favors framework ordering at the expense of polar surface sites, thereby weakening interfacial wettability and chemical anchoring ability.[38]

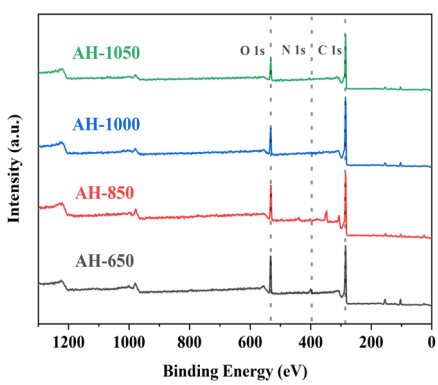

Fig. 5 XPS survey spectra of AH-650, AH-850, AH-1000, and AH-1050, showing the C 1s, O 1s, and N 1s signals and their variation with carbonization temperature.

Further insight into the evolution of surface chemistry was obtained from deconvolution of the high-resolution spectra (Fig. 6). The C 1s spectra show that the relative fraction of conductive sp^2-hybridized carbon (C=C/C–C, 284.8 eV) increases with temperature, whereas the C–O and C=O components decrease. AH-1000 reaches a relatively high sp^2-C fraction while still retaining a measurable amount of C=O groups, endowing it with both improved electronic conductivity and a moderately polar surface.[39] Mechanistically, pyridinic N and graphitic N can redistribute the local electron density of neighboring carbon atoms and strengthen the adsorption of Li_2Sn intermediates, whereas oxygen-containing groups such as C=O and C–O enhance surface polarity and electrolyte wettability, thereby favoring immobilization of polysulfides on the carbon surface rather than diffusion into the electrolyte. AH-1000 therefore achieves a better balance between conductive carbon domains and polar functional groups, enabling both electron transport and chemical confinement of polysulfides. In AH-1050, by contrast, further burn-off of polar sites weakens this interfacial anchoring function.[40] Related studies have likewise shown that heteroatom doping and carbon-microdomain engineering can accelerate electrochemical kinetics by tuning local electronic structure, defect chemistry, and ion/electron transport pathways, which is consistent with the balance observed here between framework ordering and surface polarity.[41]

3.3.2. Elemental composition analysis (EA). Elemental analysis (EA) provides direct quantitative evidence from the perspective of overall composition for the chemical evolution of the material during carbonization (Table 2). A comparison between raw cattle manure and the product carbonized at 1000 °C (AH-1000) clearly shows that high-temperature treatment causes significant changes. The most obvious changes are the sharp decreases in the mass fractions of hydrogen (H) and oxygen (O): the H content decreases markedly from 6.92% to 0.45%, and the O content drops substantially from 45.31% to 4.55%. These results quantitatively demonstrate that unstable oxygen- and hydrogen-containing functional groups as well as carbohydrate structures in the precursor undergo deep pyrolysis and aromatization during carbonization, escaping in the form of small molecules such as H_2O, CO, and CO_2. This process effectively purifies the carbon skeleton and removes a large number of unstable components that might induce side reactions in the electrochemical environment, thereby facilitating the formation of a structurally stable aromatic carbon network with enhanced conductivity.[42]

Particular attention should be paid to the retention of nitrogen (N) and sulfur (S). The N content decreases from 1.69% to 0.67%, whereas sulfur is effectively retained and even shows a certain enrichment trend. Although part of the nitrogen is lost at high temperature, AH-1000 still retains a considerable nitrogen content, about 40% of that in the raw material, while sulfur is preserved almost completely. These quantitative

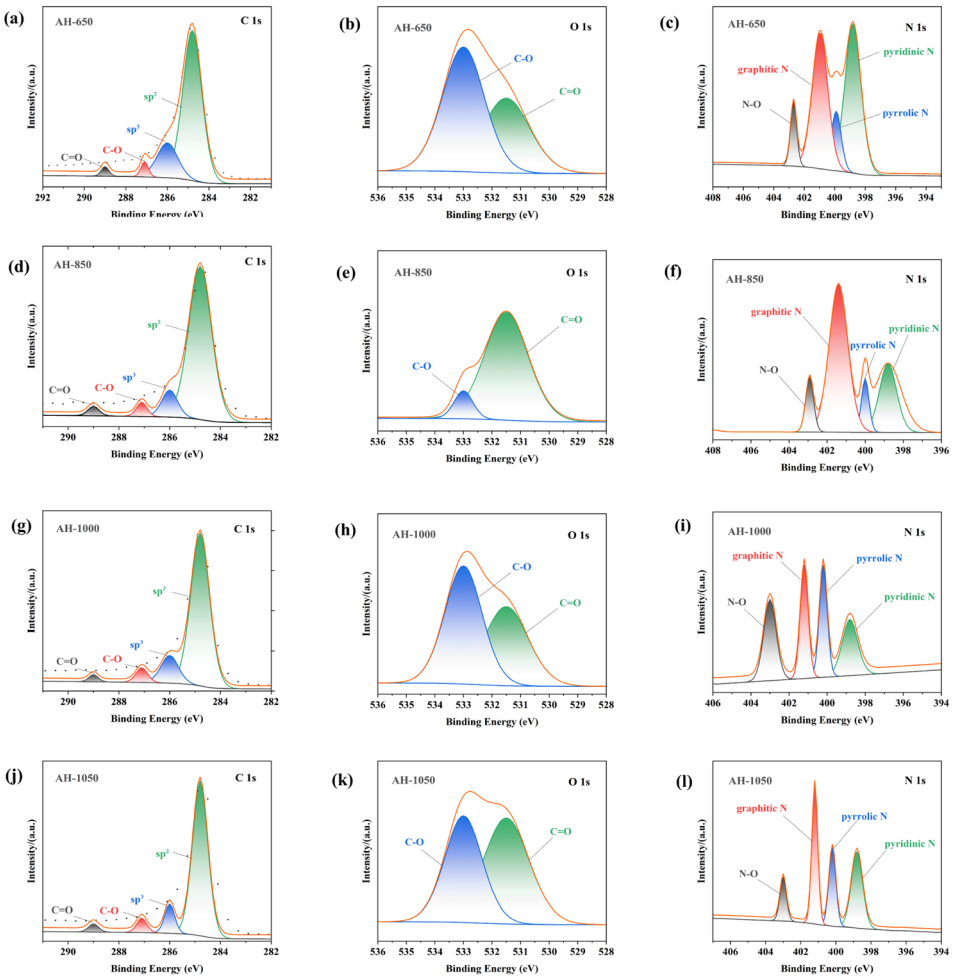

Fig. 6 High-resolution XPS spectra of cattle-manure-derived carbons: (a–c) AH-650, (d–f) AH-850, (g–i) AH-1000, and (j–l) AH-1050, showing the fitted C 1s, O 1s, and N 1s regions used to analyze carbon bonding states and surface polar functional groups.

Table 2 Elemental analysis data for the raw cattle manure and the material carbonized at 1000 °C (AH-1000)

	Element analysis (wt%)				
Sample	C	H	N	S	O
Cow dung	45.75	6.92	1.69	0.33	45.31
AH-1000	93.68	0.45	0.67	0.65	4.55

results are highly consistent with the above XPS analysis and jointly confirm that effective intrinsic N,S co-doping can be achieved when cattle manure is used as the precursor. During carbonization, relatively stable nitrogen-containing heterocycles, such as pyridinic N and graphitic N, as well as sulfur-containing structures can be retained. These heteroatoms are important for constructing chemical adsorption sites and enhancing the affinity between carbon materials and polysulfides.[43,44] Nevertheless, in absolute terms, the nitrogen content in AH-1000 remains limited. Although its chemical adsorption ability is therefore stronger than that of AH-1050, it is still insufficient to match high-performance hosts incorporating strongly polar catalytic components, which also helps explain the moderate capacity retention observed here.

3.4. Electrochemical performance and structure–property relationship

To systematically evaluate the electrochemical performance of cattle manure-derived carbons as sulfur hosts, comprehensive electrochemical tests were carried out (Fig. 7). The initial charge–discharge curves (Fig. 7a) and cyclic voltammetry (CV) curves (Fig. 7b) together reveal the intrinsic electrochemical reaction behavior of the materials.[45] Among all samples, AH-1000 exhibits the highest initial discharge specific capacity (690 mAh g^{-1}). Its CV curves also show relatively high peak currents and a smaller potential separation between the redox peaks.[46] Here, the term "best-performing" is used only within the temperature-controlled series investigated in this work, rather than as a claim of superiority over advanced catalytic or composite sulfur hosts reported in the literature. The superiority of AH-1000 arises from a more reasonable matching among its conductive framework, hierarchical pore structure, and N/O polar sites: the conductive network reduces the barrier

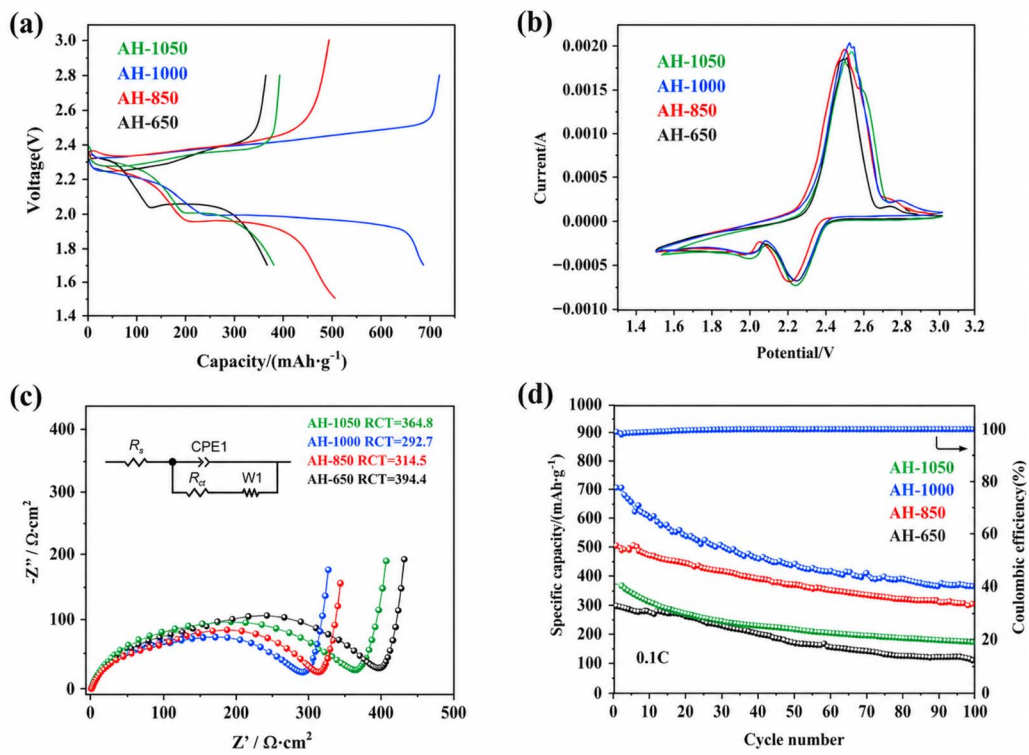

Fig. 7 Electrochemical evaluation of sulfur cathodes using cattle-manure-derived carbon hosts carbonized at different temperatures: (a) initial charge–discharge profiles, (b) cyclic voltammograms, (c) Nyquist plots with the equivalent circuit model used for impedance interpretation, and (d) cycling performance with coulombic efficiency marked on the right axis.

to electron transport, micropores and defect sites enhance the initial adsorption of sulfur species, mesopores provide space for sulfur and polysulfide migration, and the retained polar functional groups strengthen chemical anchoring.

Electrochemical impedance spectroscopy (EIS, Fig. 7c) further supports the above structure–property relationship from the perspective of interfacial kinetics.[47] AH-1000 exhibits a relatively smaller high-frequency semicircle, indicating a comparatively smoother charge-transfer process. Cycling tests (Fig. 7d) show that AH-1000 retains the best performance within 100 cycles, but the cycle number remains limited and the long-term retention still leaves room for improvement. The main causes of the remaining decay include the limited specific surface area and pore volume of the samples, insufficient physical confinement of sulfur and polysulfides, the absence of catalytic sites that could accelerate polysulfide conversion, and the continued occurrence of shuttle-related active-material loss during cycling.

From the structure–property perspective, the suppression of polysulfides in this system mainly originates from the synergy of three aspects: first, the three-dimensional interconnected carbon skeleton provides continuous electron-transport pathways; second, micropores, defect sites, and relatively tortuous channels produce physical confinement of polysulfides; third, the retained N/O polar sites offer chemical anchoring toward soluble Li_2Sn intermediates. Although this conductivity-confinement-anchoring synergy makes AH-1000 the best-performing sample in the temperature series, its capacity and cycling stability still remain at a moderate level compared with advanced sulfur hosts that employ heteroatom/polar-site engineering, shuttle-effect suppression strategies, or catalytic Ni–N4 centers.[12,15,16] Therefore, based on the current limitations in pore development, polar-site retention, and sulfur-redox kinetics, further optimization of cattle-manure-derived carbon hosts should focus on cost-controlled pore regulation, stabilization of surface polar sites during carbonization, and the introduction of inexpensive catalytic components to enhance polysulfide confinement and conversion.

4. Conclusions

Cattle manure is an abundant livestock waste that causes disposal pressure when improperly treated, but its carbon-rich composition and inherent heteroatoms also make it a promising low-cost precursor for functional carbon materials. In this study, cattle manure was converted into carbon hosts for lithium–sulfur batteries through a unified pretreatment route followed by carbonization at different temperatures. By keeping the precursor treatment unchanged and only varying the carbonization temperature, the temperature-dependent evolution of morphology, carbon-framework ordering, pore structure, surface chemistry, and electrochemical behavior was systematically clarified.

Among the obtained samples, AH-1000 showed the most favorable balance between a three-dimensional conductive carbon framework, relatively preserved pore structure, and moderate retention of N/O polar sites. XRD and Raman analyses confirmed that increasing carbonization temperature promoted local graphite-like ordering, whereas excessive temperature reduced defect density and surface-active sites. BET results further showed that the pore structure remained modest overall, and XPS/EA results demonstrated that part of the intrinsic heteroatoms could be retained after carbonization. Benefiting from this balanced structure, AH-1000 delivered the highest initial discharge capacity of 690 mAh g^{-1} at 0.1C and showed the best cycling response within the temperature series. However, compared with highly activated or catalytically modified sulfur hosts, the present cattle-manure-derived carbons still suffer from limited specific surface area, insufficient pore development, partial loss of polar sites, and the absence of catalytic components, which restrict their sulfur-storage capability and long-term stability.

Overall, this work demonstrates the feasibility of converting cattle manure from a low-value waste into carbon hosts for lithium–sulfur batteries and establishes a structure–performance basis for this biomass-derived carbon system. Future optimization should focus on cost-controlled pore regulation, stabilization of surface polar sites during carbonization, introduction of inexpensive catalytic components, simplification of the pretreatment process, and electrochemical evaluation under higher sulfur loading and lean-electrolyte conditions. These improvements may further enhance the practical value of cattle-manure-derived carbon materials while maintaining the resource-utilization significance of the proposed route.

Author contributions

Peng Li: conceptualization, investigation, funding acquisition, data curation, writing–original draft. Yingjie Liu: methodology, validation. Yongzhen Ma: validation. Zhicheng Zhao: validation. Zheng Zhang: resources.

Conflicts of interest

The authors affirm that they have no known competing financial interests or personal relationships that might have potentially exerted influence on the research outcomes presented in this paper.

Data availability

The data that support the findings of this study are available from the corresponding author upon reasonable request.

Supplementary information (SI) is available. See DOI: https://doi.org/10.1039/d6ra01639a.

Acknowledgements

This work was supported by the Natural Science Foundation of Shanxi Province (No. 202403021222190). Shanxi Provincial College Students' Innovation Training Program (No. 20250921). The authors express gratitude to Dr Jin Chang for his guidance on the article and thank Wen Li for assisting in the experimental validation.

References

1 Y. L. Bai, C. C. Zhang, F. Rong, *et al.*, Biomass-derived carbon materials for electrochemical energy storage, *Chem. – Eur. J.*, 2024, **30**(23), e202304157.
2 H. He, R. Zhang, P. Zhang, *et al.*, Functional carbon from nature: biomass-derived carbon materials and the recent progress of their applications, *Adv. Sci.*, 2023, **10**(16), 2205557.
3 P. Zhang, Y. Li, Y. Liu, *et al.*, Heteroatom-Enriched Multiscale Porous Carbon from Semen Cassiae for High-Energy Supercapacitors, *Renew. Energy*, 2026, 125270.
4 Y. Chen, X. Li, K. Park, *et al.*, Nitrogen-doped carbon for sodium-ion battery anode by self-etching and graphitization of bimetallic MOF-based composite, *Chem*, 2017, **3**(1), 152–163.
5 C. Choi, Y. Luo, A. Reed, *et al.*, Hybrid materials for electrochemical energy storage, *Chem. Mater.*, 2024, **36**(24), 11738–11755.
6 P. Guo, R. Xue, Q. Zou, *et al.*, Enhanced ultramicropore of biomass-derived porous carbon for efficient and low-energy CO2 capture: integration of adsorption and solar desorption, *Energy Environ. Mater.*, 2025, e70140.
7 F. Hu, H. Yang, X. Zhou, *et al.*, Spatial dynamics of lithium battery recycling enterprises in China: implications for smart waste management and public health, *Front. Public Health*, 2026, **13**, 1729413.
8 Y. Ma, X. Jin, Y. Hu, *et al.*, Recovery of hydrogen and sulfur by electrolysis of ionized H2S in an amine-containing organic electrolyte with highly temperature-dependent sulfur solubility, *Energy Fuels*, 2020, **34**(6), 7756–7762.
9 G. Xu and Z. Yang, Risk-aware low carbon optimization of hydrogen-oriented multi-energy system with linear approximation of bi-product fuel cell, *Energy*, 2025, **334**, 137581.
10 Y. Jiao, K. Xu, H. Xiao, *et al.*, Biomass-derived carbon aerogels for ORR/OER bifunctional oxygen electrodes, *Nanomaterials*, 2023, **13**(17), 2397.
11 Y. Li, Z. Wang, Q. Zhang, *et al.*, Lightweight Materials for High Energy Density Lithium-Sulfur Batteries, *Adv. Energy Mater.*, 2025, **15**(19), 2406069.
12 J. Wang and W. Q. Han, A review of heteroatom doped materials for advanced lithium-sulfur batteries, *Adv. Funct. Mater.*, 2022, **32**(2), 2107166.
13 Q. Li, Y. Liu, Y. Wang, *et al.*, Review of the application of biomass-derived porous carbon in lithium-sulfur batteries, *Ionics*, 2020, **26**(10), 4765–4781.
14 Z. Zhu and Z. Xu, The rational design of biomass-derived carbon materials towards next-generation energy storage: A review, *Renewable Sustainable Energy Rev.*, 2020, **134**, 110308.
15 J. Li, L. Gao, F. Pan, *et al.*, Engineering strategies for suppressing the shuttle effect in lithium-sulfur batteries, *Nano-Micro Lett.*, 2024, **16**(1), 12.

16 H. Zhang, Y. Meng, F. Wang, *et al.*, Dynamic Ni-N4 centers enable concurrent polysulfide catalysis and Li^+ flux control for high-performance Li-S batteries, *AIChE J.*, 2026, **72**(2), e70130.
17 W. Hao, F. Guo, J. Li, *et al.*, Influence of Physical Parameters on Lithium Dendrite Growth Based on Phase Field Theory, *Metals*, 2025, **16**(1), 41.
18 T. Long and Y. Guo, Research on the temperature radius stratification model based on electrochemical-thermal-force coupling in lithium-ion batteries, *Electrochem. Commun.*, 2025, **180**, 108052.
19 G. Xu, State-of-charge estimation method for lithium-ion batteries based on competitive SIR model, *Front. Energy Res.*, 2022, **10**, 984107.
20 B. Song, L. Su, X. Liu, *et al.*, An examination and prospect of stabilizing Li metal anode in lithium-sulfur batteries: a review of latest progress, *Electron*, 2023, **1**(2), e13.
21 H. Zhang, X. Li,and H. Zhang, in *Li-S and Li-O_2 Batteries with High Specific Energy: Research and Development*, 2016, pp. 1–48.
22 Z. W. Seh, Y. Sun, Q. Zhang, *et al.*, Designing high-energy lithium-sulfur batteries, *Chem. Soc. Rev.*, 2016, **45**(20), 5605–5634.
23 Q. Pang, X. Liang, C. Y. Kwok, *et al.*, Advances in lithium-sulfur batteries based on multifunctional cathodes and electrolytes, *Nat. Energy*, 2016, **1**(9), 1–11.
24 J. Zhang, H. Huang, J. Bae, *et al.*, Nanostructured host materials for trapping sulfur in rechargeable Li-S batteries: structure design and interfacial chemistry, *Small Methods*, 2018, **2**(1), 1700279.
25 G. Li, S. Wang, Y. Zhang, *et al.*, Revisiting the role of polysulfides in lithium-sulfur batteries, *Adv. Mater.*, 2018, **30**(22), 1705590.
26 X. Chen, H. J. Peng, R. Zhang, *et al.*, An analogous periodic law for strong anchoring of polysulfides on polar hosts in lithium sulfur batteries: S-or Li-binding on first-row transition-metal sulfides, *ACS Energy Lett.*, 2017, **2**(4), 795–801.
27 Q. Zhao, Q. Zhu, Y. Liu, *et al.*, Status and prospects of MXene-based lithium-sulfur batteries, *Adv. Funct. Mater.*, 2021, **31**(21), 2100457.
28 Z. Sun, J. Zhang, L. Yin, *et al.*, Conductive porous vanadium nitride/graphene composite as chemical anchor of polysulfides for lithium-sulfur batteries, *Nat. Commun.*, 2017, **8**(1), 14627.
29 B. Lesbayev, M. Auyelkhankyzy, G. Ustayeva, *et al.*, Recent advances: Biomass-derived porous carbon materials, *S. Afr. J. Chem. Eng.*, 2023, **43**(1), 327–336.
30 S. Huang, Z. Wang, Y. Von Lim, *et al.*, Recent advances in heterostructure engineering for lithium-sulfur batteries, *Adv. Energy Mater.*, 2021, **11**(10), 2003689.
31 L. Chen, H. Yu, W. Li, *et al.*, Interlayer design based on carbon materials for lithium-sulfur batteries: a review, *J. Mater. Chem. A*, 2020, **8**(21), 10709–10735.
32 L. Zhang, D. Liu, Z. Muhammad, *et al.*, Single nickel atoms on nitrogen-doped graphene enabling enhanced kinetics of lithium-sulfur batteries, *Adv. Mater.*, 2019, **31**(40), 1903955.
33 J. Xu, W. Zhang, H. Fan, *et al.*, Promoting lithium polysulfide/sulfide redox kinetics by the catalyzing of zinc sulfide for high performance lithium-sulfur battery, *Nano Energy*, 2018, **51**, 73–82.
34 F. Han, D. Yan, X. Guan, *et al.*, Self-assembled 3D CoSe-based sulfur host enables high-efficient and durable electrocatalytic conversion of polysulfides for flexible lithium-sulfur batteries, *Energy Storage Mater.*, 2024, **71**, 103652.
35 C. Ma, M. Zhang, Y. Ding, *et al.*, Green production of biomass-derived carbon materials for high-performance lithium-sulfur batteries, *Nanomaterials*, 2023, **13**(11), 1768.
36 Q. Zhang, Q. Huang, S. M. Hao, *et al.*, Polymers in lithium-sulfur batteries, *Adv. Sci.*, 2022, **9**(2), 2103798.
37 X. Chen, T. Hou, K. A. Persson, *et al.*, Combining theory and experiment in lithium-sulfur batteries: Current progress and future perspectives, *Mater. Today*, 2019, **22**, 142–158.
38 R. Yan, M. Oschatz and F. Wu, Towards stable lithium-sulfur battery cathodes by combining physical and chemical confinement of polysulfides in core-shell structured nitrogen-doped carbons, *Carbon*, 2020, **161**, 162–168.
39 J. Sun, L. Ye, X. Zhao, *et al.*, Electronic modulation and structural engineering of carbon-based anodes for low-temperature lithium-ion batteries: a review, *Molecules*, 2023, **28**(5), 2108.
40 H. Shi, W. Sun, J. Cao, *et al.*, Challenges and solutions for lithium-sulfur batteries with lean electrolyte, *Adv. Funct. Mater.*, 2023, **33**(42), 2306933.
41 M. Bartoli, A. Piovano, G. A. Elia, *et al.*, Pristine and engineered biochar as Na-ion batteries anode material: A comprehensive overview, *Renewable Sustainable Energy Rev.*, 2024, **194**, 114304.
42 Y. Wang, Y. Wang, L. Zhang, *et al.*, Exogenous phosphorus supplementation and sodium reduction treatment to realize N, P co-doped hard carbon with reduced oxygen-containing groups for high-performance sodium-ion batteries, *J. Power Sources*, 2025, **630**, 236156.
43 B. Tang, Y. Zhang, B. Ji, *et al.*, Ion-mediated carbon microdomain engineering boosting enhanced plateau capacity of carbon anode under high rate towards high-performance sodium dual-ion batteries, *Nano-Micro Lett.*, 2026, **18**, 161.
44 Y. Wang, L. Zhang, H. Hou, *et al.*, Recent progress in carbon-based materials for supercapacitor electrodes: a review, *J. Mater. Sci.*, 2021, **56**(1), 173–200.
45 Z. Ma, K. Wang, Y. Qiu, *et al.*, Nitrogen and sulfur co-doped porous carbon derived from bio-waste as a promising electrocatalyst for zinc-air battery, *Energy*, 2018, **143**, 43–55.
46 W. Wei and P. Liu, Rational porous design for carbon nanotubes derived from tubular polypyrrole as sulfur host for lithium-sulfur batteries, *Microporous Mesoporous Mater.*, 2021, **311**, 110705.
47 S. Waluś, C. Barchasz, R. Bouchet, *et al.*, Electrochemical impedance spectroscopy study of lithium-sulfur batteries: Useful technique to reveal the Li/S electrochemical mechanism, *Electrochim. Acta*, 2020, **359**, 136944.